SINGLE MASK, LARGE FORCE, AND LARGE DISPLACEMENT ELECTROSTATIC LINEAR INCHWORM MOTORS

Richard Yeh, Seth Hollar, and Kristofer S. J. Pister
Berkeley Sensor and Actuator Center
Dept. of Electrical Engineering and Computer Science
University of California, Berkeley, CA 94720

ABSTRACT

We have demonstrated a family of large force and large displacement electrostatic linear inchworm motors that can operate with moderate to high voltages. The inchworm motor design decouples actuator force from total travel and allows the use of electrostatic gap-closing actuators to achieve large force and large displacement while consuming low power. A typical inchworm motor measures 3mm x 1mm x 50µm and can lift over 130 times its own weight. One motor has achieved a travel of 80µm and a calculated force of 260µN at 33V. The force density of that motor was 87µN/mm^2 at 33V and the energy efficiency was estimated at 8%. Another motor displaced the shuttle at an average velocity of almost 4mm/s and achieved an estimated power density of 190 W/m^3. Motors were cycled 23.6 million times for over 13.5 hours without stiction. This family of motors is fabricated on Silicon-on-Insulator wafers using only a single mask.

INTRODUCTION

MEMS applications often require large force, large displacement, and low-power actuators. One example would be autonomous microrobots which require hundreds of µN of force, tens of µm of travel, and must power actuators and electronics from onboard energy sources. However, most MEMS actuators either have a force-displacement trade-off or simply have small displacements. In addition, many actuators, such as those based on thermal or magnetic principles, consume high power (> tens of mW). In 1995, we demonstrated the first MEMS electrostatic linear inchworm motor [1]. This motor achieved moderate displacement by accumulating smaller displacements over time. Also, these motors made use of electrostatic gap-closing actuators (GCA), which possess high force densities at small displacements and consume low power (tens of µW).

Fig. 1 compares the estimated force-densities and travel of several published MEMS motors. Our first inchworm motor was fabricated in MUMPS which provides thin-film (1.5-2µm) polysilicon. The process has an aspect ratio of 2 which limits the force density of the motor. In addition, the stress gradient inherent in LPCVD polysilicon films limits the overall size of the motors. In 1997, Baltzer et. al. [2] reported a GCA inchworm motor fabricated in a similar process. It had a larger travel but the force density was still low. Saif et. al. [3] demonstrated a high aspect-ratio millimeter-sized comb-drive actuator which produced a high force density but had limited travel. The Sandia Microengine [4] used a low aspect ratio comb-drive actuator which produced a low force density but, with its gear trains, achieves large travel and large torque. The motors presented in this paper are fabricated in Silicon-on-Insulator (SOI) wafers with an aspect ratio of up to 25:1. This enables us to achieve a theoretical force density of approximately 1mN/mm^2 at 30V. Other MEMS motors with similar force densities are the thermal inchworm motor [5] and the scratch drive actuator [6]. However, both of these motors are extremely inefficient and thus would not be appropriate for most autonomous applications.

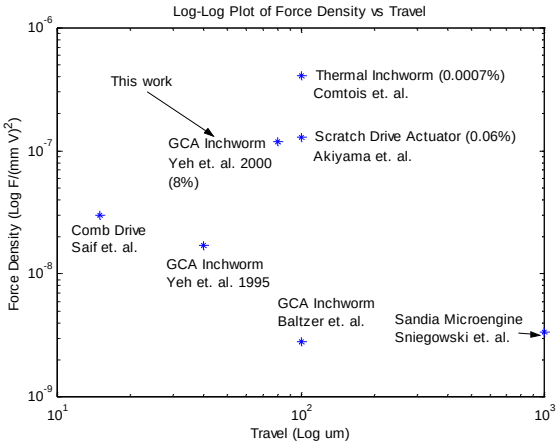

Fig. 1. A log-log plot of the force densities normalized to the voltage squared vs. the stroke of several motors [1-6]. Energy efficiency in parenthesis.

INCHWORM MOTOR DESIGN

The inchworm motor consists of two x-y actuators and a sliding shuttle (Fig. 2). The x-y actuator consists of a pawl connected to two orthogonal sets of actuator arrays. To move the shuttle, the pawl engages the shuttle using the clutch-GCA array and then pushes or pulls the shuttle using the drive-GCA array. During the inchworm cycle, the two x-y actuators alternately move the shuttle to accumulate large displacements incrementally (Fig. 3). This

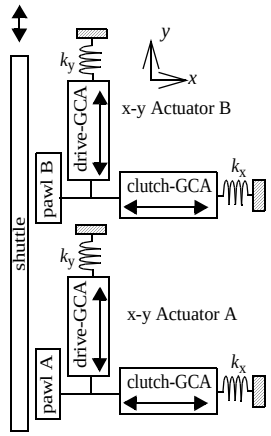

Fig. 2. Diagram of a linear inchworm motor.

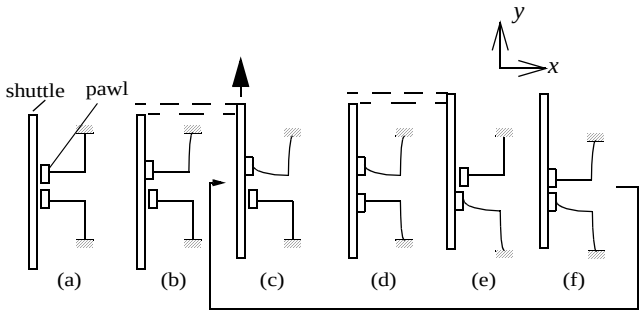

Fig. 3. Diagram of an inchworm cycle. (a) pawls at initial position. (b) pawl B attaches to shuttle. (c) pawl B pulls shuttle. (d) pawl A attaches to and holds shuttle. (e) pawl B detaches from shuttle as pawl A pulls the shuttle. (f) pawl B attaches and holds the shuttle. repeat from step (c).

technique decouples the actuator force from maximum displacement. The resolution of the displacement is defined and limited by the lithography and aspect ratio of the fabrication process.

ACTUATOR DESIGN

The gap-closing actuator (GCA) consists of two parallel beams of length, *l*, and thickness, *t*, separated by a gap, g_1. One beam is anchored to the substrate while the other is supported by a spring. When a voltage is applied between the two beams, an electric field in the gap causes the spring-supported beam to move towards the stationary beam. To prevent shorting between the two beams, an anchored gap-stop biased at the same potential as the supported beam is used. The gap between the gap-stop and the supported beam, g_3 is less than g_1. This gap, g_3, defines the step size of the motor. To generate more force, an array of GCA's are used in the motor. Fig. 4 shows the diagram of an array of two GCA's separated by a gap of, g_2.

ANALYSIS

Now we can examine the one dimensional dynamic analysis of the moving GCA array. We consider the following forces in our model:

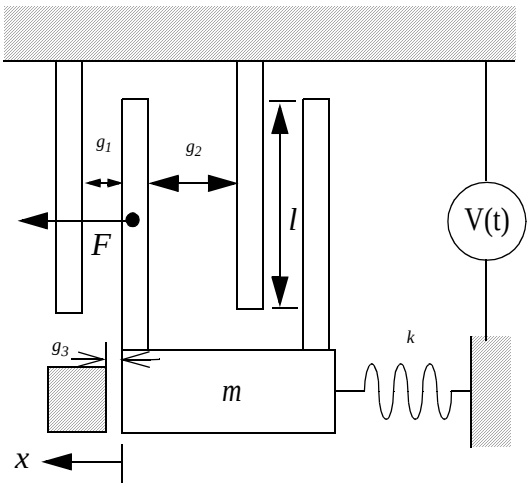

Fig. 4. Diagram of an array of two gap-closing actuators.

$$m\ddot{x} = F_{e1} + F_{e2} + F_s + F_{sq} + F_L \quad (1)$$

where F_{e1}, F_{e2} are the electrostatic forces acting from the left and right sides of the beam (Fig. 4), respectively, F_s, is the spring restoring force, and F_{sq} is the squeeze film damping forces again, acting from the left and right sides, respectively. F_L is the load.

The electrostatic force, F_{e1}, between the two beams in a GCA is given by:

$$F_{e1} = \frac{1}{2}\varepsilon N V_{app}^2 \frac{tl}{(g_1 - x)^2} = \frac{k_e}{(g_1 - x)^2} \quad (2)$$

where g_1 is the initial gap distance between the two GCA beams, V_{app} is the applied potential across the two beams, *t* is the thickness of the beam, *l* is the overlapping length of the beams, ε is the permittivity of air, N is the number of GCA's in the array, and *x* is the position of the moving beam. Likewise the parasitic electrostatic force, F_{e2}, between the moving beam of one GCA and the stationary beam of the next GCA has a similar equation. To maximize the force density of the GCA array, g_2 is chosen to be close to be 2.8 times g_1. The restoring force of the support springs for the moving beams is given by Hooke's Law. The fourth force in our model is due to squeeze film damping. The force becomes significant when the gap between the beams become small compared to the length and thickness of the beams. The following damping force equation is based on Starr [7]:

$$F_{sq} = -\frac{N\left(1 - 0.6\frac{t}{l}\right)t^3 l\mu}{(g_1 - x)^3}\dot{x} = \frac{-b\dot{x}}{(g_1 - x)^3} \quad (3)$$

where μ is the viscosity of air and $t < l$. Substituting Eqn. 2 and 3 into Eqn 1, we have the 1-D dynamics equation for the supported beam:

$$m\ddot{x} + \frac{b\dot{x}}{(g_1 - x)^3} + k_s x = k_e\left(\frac{1}{(g_1 - x)^2} - \frac{1}{(g_2 - x)^2}\right) + F_L \quad (4)$$

Below is the pull-in voltage, V_{pi}, which is the *minimum* voltage required to close the gap with no external load:

$$V_{pi} = \sqrt{\frac{8}{27}\frac{k_s g_1^3}{\varepsilon t^3 l N}} \quad (5)$$

Speed

The maximum frequency of operation for the GCA inchworm motors is limited by the time it takes to close (pull-in) and open (pull-out) the gap. Eqn. 4 can be solved numerically for the position, *x(t)*. Fig. 5 shows the position as a function of time for pull-in and pull-out. From Fig. 5, the cycle time is equal to the summation of T_1 to T_4. Since T_1 is equal to T_3 and T_2 is equal to T_4, the cycle time is equal to:

$$T = 2(T_1 + T_2) \quad (6)$$

The minimum T_1 is determined by the pull-in time of the clutch A and the minimum T_2 is determined by the maximum of the pull-in

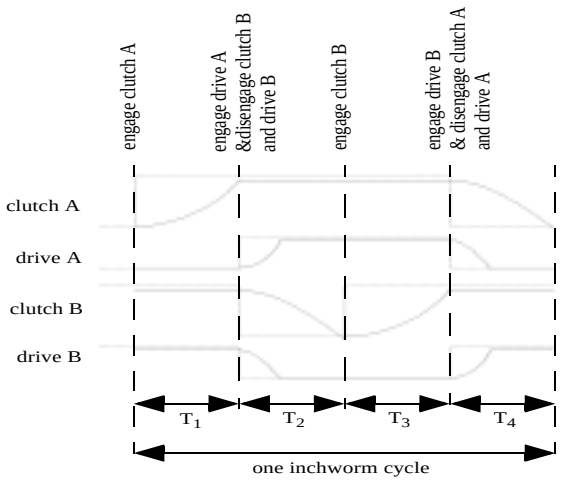

Fig. 5. Timing diagram for the inchworm motor through one cycle. The dotted lines indicate the drive signals and the solid lines indicate simulated responses of the beam positions.

time of drive A, pull-out time of clutch B, and pull-out time of drive B.

The analysis of the inchworm motors has shown that the minimum times, T_1 and T_2, depend on the clutch engagement (pull-in) and disengagement (pull-out) times, respectively. According to the model, the pull-in time can be decreased by increasing the applied voltage as it is proportional to $1/V^2$ and the pull-out time can be decreased by increasing the spring constant as it is proportional to $\sqrt{1/k}$ according to the model.

Scaling Effects

The effect as all dimensions, λ, are scaled down isotropically is shown in Table 1. Details are described in [9]. The GCA scales favorably as the minimum feature size decreases.

Unit	Scaling
Electrostatic Force	λ^2
Natural Frequency	$1/\lambda$
Squeeze film damping force	λ
Power Density	$1/\lambda$

The only non-intuitive scaling effect above is in the electrostatic force which scales as λ^2. This is because catastrophic pull-in and shorting of GCA beams forces voltage scaling as a fixed design geometry is scaled [10]. Above this maximum V_{pi}, the GCA beams will be non-rigid as they bend towards each other and make contact.

Power

The power dissipated by the inchworm motor is:

$$P = CV^2 \cdot f \tag{7}$$

where C is the total capacitance of the motor:

$$C = C_{drive} + C_{clutch} + C_{parastics} \tag{8}$$

and f is the frequency of operation. As expected, there is a trade-off between speed and the power dissipated. The only capacitance to

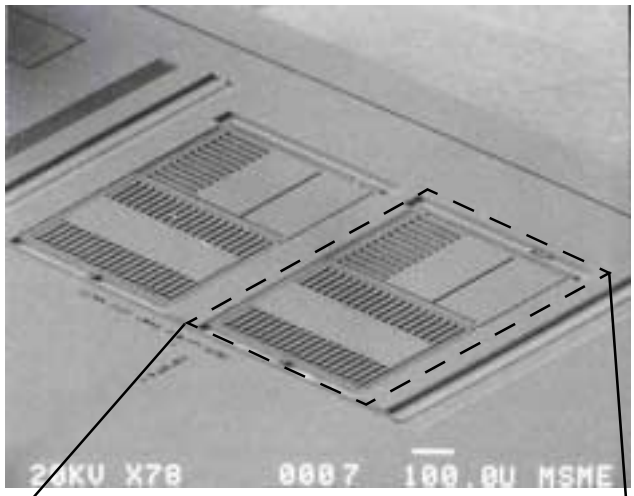

(a)

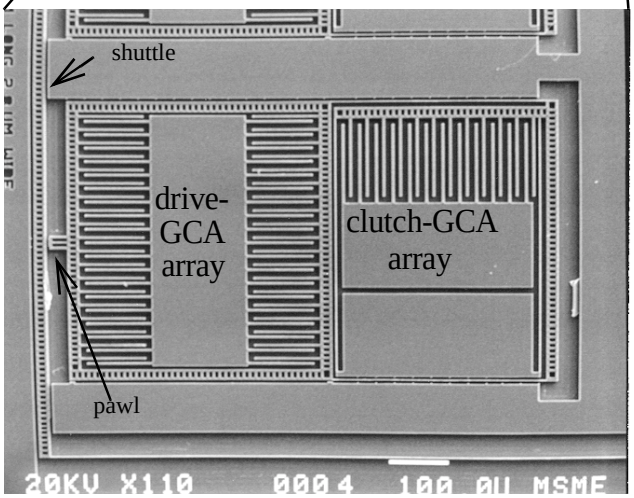

(b)

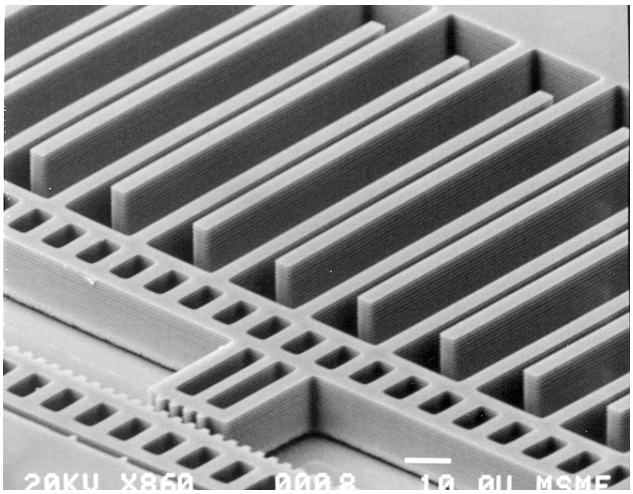

(c)

Fig. 6. (a) SEM of an inchworm motor fabricated on an SOI wafer. This motor displaced the shuttle by 48μm in 12 cycles. The displacement was limited only by this particular shuttle design (not force-limited). (b) SEM close-up of the x-y actuator and pawl. Note the arrays of gap-closing actuators.(c) SEM close-up of the clutch-GCA array, pawl, and shuttle.

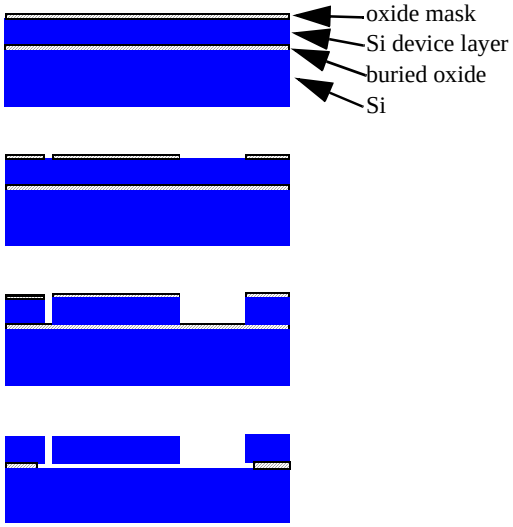

Fig. 7. Single-Mask fabrication process. (a) Oxidize wafer to create mask layer. (b) pattern oxide. (d) etch Si. (e) HF etch of Si.

produce work on the load is C_{drive}. Therefore, to reduce power dissipation and to increase the power efficiency, C_{clutch} and $C_{parasitics}$ need to be minimized. C_{clutch} is directly proportional to the clutch GCA array size which can be reduced by minimizing the width of the beams supporting the clutch GCA array (reducing V_{pi}) and adding gear teeth on the pawl and shuttle. The pulling force of the motor can be limited by the force required to break the engagement of the pawl and shuttle. Motors in [1, 2] used friction from the smooth sidewalls of the pawl and shuttle as an engagement force. The clutch then had to have a large pull-in force to maintain static engagement of the shuttle. Our current motors incorporate gear teeth on the pawl and shuttle and therefore, do not require any frictional force to prevent slipping. The engagement is only set by the V_{pi} of the clutch GCA. The source of $C_{parasitics}$ are between the bonding pads and the substrate. To reduce $C_{parasitics}$, we use SOI wafers with the thickest buried oxide layer available (~2µm) and minimize the bond pad areas.

To produce 1.5mN of force using a 30V supply and a 3µm initial gap in the GCA's, an initial GCA capacitance of 10pF is needed. If the final gap is one third of the initial gap, then the final GCA capacitance will be three times the initial capacitance. If we operate the GCA at 1kHz, then the power dissipated in the x-y actuator will be only 75µW, with an output power of 6µW.

FABRICATION

The inchworm motors were fabricated by the following process (Fig. 7). We start with a SOI wafer that has a top layer silicon thickness of 15 - 50µm, a buried oxide layer of 2µm, and a silicon handle wafer. A 0.5µm-thick oxide masking layer is thermally grown on the wafer. The masking layer is patterned by the single mask and then photoresist (PR) is removed to prevent PR from being hardened in the silicon etch. The exposed areas are etched down to the buried oxide. The wafer is diced and then the sacrificial oxide layer is removed in a timed etch that allows moving structures to be released while anchored structures maintain the oxide underneath. To reduce release stiction, the wafer is dried in a critical point dryer (CPD). After mounting the chip to a package, wires are bonded directly to bare silicon pads on the chip to actuate the motors.

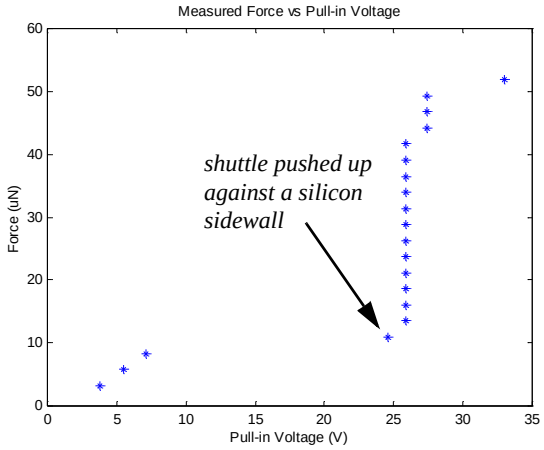

Fig. 8. Measured force vs. pull-in voltage as the shuttle is displaced by 80µm in 2µm increments. The discontinuity occurred when the shuttle was pushed laterally against a silicon sidewall by the clutch-GCA.

RESULTS

Using a single mask to define the motors, we have fabricated and tested several versions of the inchworm motor. The etch was done with a commercial deep trench etcher with an aspect ratio of 25:1. An SEM micrograph of one of the inchworm motors fabricated is shown in Fig. 6. The motor dimension is 1.5mm x 1mm x 15µm on a silicon handle wafer. A similar motor with a travel of 52µm was operated at a maximum frequency of 1kHz, moving the shuttle by an average velocity of 4mm/s. The theoretical frequency limit according to our model is 1.4kHz. Experimentally, we measured the minimum timing T_1 as 0.16 milliseconds and T_2 as 0.35 milliseconds. Our theoretical results predict 0.17 milliseconds and 0.18 milliseconds for T_1 and T_2, respectively. While the data matches well for T_1, T_2 differs by about a factor of two. Possible reasons for extended cycle period could include extra time to disengage from the shuttle and actuator bouncing against gap stops. At this frequency, the power density of this motor is estimated at 190 W/m^3. At higher speeds, some slipping between the pawls and the shuttle was observed.

Another version of the motor with dimensions of 1.5mm x 2mm x 50µm on a silicon substrate was demonstrated with a travel of 80µm and exerted a measured force of over 50µN in *excess* of the friction it overcame. The force was measured by the displacement of the shuttle supporting springs. Fig. 8 shows the measured force vs. V_{pi} as the shuttle is displaced by 80µm in 2µm step sizes. During operation, the shuttle was displaced laterally by the force of the clutch and subsequently pushed against the silicon side wall on the other side of the shuttle (Fig. 6c). The drive-GCA was nevertheless able to overcome the sidewall friction and pull the shuttle forward. The force generated, estimated by the *Vpi* required to displace the shuttle to 80µm was 260µN at 33V. The force density achieved is 87µN/mm^2. The theoretical upper limit of the force density at 33V and an aspect ratio of 25:1 is approximately 1mN/mm^2. This implies our motors have a fill factor of around 11% as the rest of the area is occupied by support structures, bonding pads,

etc. Motors were operated for over 13.5 hours for a total of 23.6 million cycles without stiction.

SUMMARY AND DISCUSSION

Electrostatic gap-closing actuators provide respectable force densities. These densities improve as lithographic limits decrease and anisotropic etch aspect ratios increase. GCA's are also limited in travel, so their large forces can only be applied over short distances. Fortunately, one GCA can be used to drive a clutch, allowing a second GCA to make intermittent contact with a moving shuttle. Repeated cycling through the gripping/pulling/releasing sequence generates large displacements while maintaining the full force available from the GCA primary using an inchworm-like motion.

Early problems with the electrostatic inchworm motors were related to clutch slipping, and clutch and gap-stop adhesion. The former problem has been addressed by using a sawtooth shape on the shuttle and clutch, and the latter by using a thicker SOI rather than thinner polysilicon structural layer. It is not clear why the adhesion problems have disappeared in the thicker single crystal silicon. The surface roughness of the sidewalls due to a DRIE etch may decrease the adhesion force, or the adhesion force may be relatively independent of film thickness, while the restoring force due to the support springs increases linearly with thickness.

We have demonstrated motors with 80 microns of motion, stepping rates of 1000 full steps/second corresponding to 4mm/s shuttle velocity, and hundreds of uN of force. In all cases, displacement was limited by contact with a physical constraint (spring travel limits, nearby structures, etc.) rather than an intrinsic limit.

The motors presented here are based on 2 micron lithography, with most features 3 microns or larger. Based on a simple dynamic model, it appears that these designs could be directly scaled down by a factor of 3 without a decrease in actuation voltage, and without seeing serious squeeze-film damping effects. Such a scaled motor would have the same force output, and the same velocity (smaller, faster steps), but only one tenth the layout area. Deep sub-micron scaling with this exact design will necessitate voltage scaling, but a careful mechanical re-design should enable motors that are ultimately limited by field emission from the GCA's, rather than destructive pull-in.

For micro robot applications, the energy efficiency of these motors is very attractive. While the 8% efficiency demonstrated is workable, the practical limits of an inductively charged, constant-charge GCA with similar mechanical power output should be closer to 80%. In addition, a motor with dimensions of 3mm x 1mm x 50µm can lift over 130 times its own weight with 33V. The inchworm motion of the motors with near-zero static power consumption is also attractive for solar powered bugs of the future, which may need to integrate charge for many milliseconds before each phase of motor actuation.

REFERENCES

[1] R. Yeh, E. Kruglick, and K.S.J. Pister, "Microelectromechancial Components for Articulated Microrobots", Proc. The Eighth International Conference on Sensors and Actuators (Transducers '95), Stockholm, Sweden, June 25-29, 1995, pp. 346-349.

[2] M. Baltzer, T. Kraus, and E. Obermeier, "A linear stepping actuator in surface micromachining technology for low voltages and large displacements," Transducers' 97, pp. 781-4, Vol. 2.

[3] M.T.A Saif and N. MacDonald, "A millinewton microloading device," Transducers' 95, pp. 60-3, Vol. 2.

[4] E.J. Garcia and J.J. Sniegowski, "Surface Micromachined Microengine," Sensors and Actuators A (Physical), Vol. A48, no. 3, pp. 203-14.

[5] J. Comtois and V. Bright, "Applications for surface-micromachined polysilicon thermal actuators and arrays," Sensors and Actuators A (Physical), Vol. A58, no. 1, pp. 19-25.

[6] T. Akiyama and H. Fujita, "A quantitative analysis of Scratch Drive Actuator using buckling motion," MEMS '95, pp. 310-15.

[7] Starr, J.B., "Squeeze-film damping in solid-state accelerometers," IEEE Proc. Solid State Sensor and Actuator Workshop, Hilton Head, South Carolina, June 4-7, 1990, pp. 44-47.

[8] Chu, P.B., and Pister, K.S.J., "Analysis of closed-loop control of parallel-plate electrostatic microgrippers," Proc. IEEE International Conference on Robotics and Automation, San Diego, California, May 8-13, 1994, vol.1, pp. 820-5.

[9] R. Yeh and K.S.J. Pister, "Design of Low-Power Articulated Microrobots," Proc. International Conference on Robotics and Automation, Workshop on Mobile Micro-Robots, San Francisco, April 23-28, 2000, pp. 21-28.

[10] P.M. Osterberg and S.D. Senturia, "M-Test: A test chip for MEMS material property measurement using electrostatically actuated test structures," Journal of Microelectromechanical Systems, Vol. 6, No. 2, June 1997, pp. 107-118.

[11] B. Atwood, B. Warneke, and K.S.J. Pister, "Preliminary circuits for smart dust," to be presented at the IEEE 2000 Southwest Symposium on Mixed-Signal Design, Feb. 27-29, 2000, San Diego, CA, USA.